Boletim da Sociedade Astronômica Brasileira, **34**, no. 1, 106-110

Analysis of the orbital profile of populations of galaxies in clusters

G. A. Valk[1] & S. B. Rembold[1]

[1] Universidade Federal de Santa Maria, RS, Brazil e-mail: greique.valk@acad.ufsm.br, sandro.rembold@ufsm.br

Abstract. Galaxies have different shapes and properties, as well as a natural tendency to clump together gravitationally to form groups and clusters. Currently it is known that the environment of clusters can change the morphology and properties of galaxies through several processes. Thus, we expect a relation between orbital evolution of a population and its state of relaxation in the cluster. Consequently, studying the orbits of galaxies can offer us information about the environmental processes that occur in the intracluster environment. In this work, using a sample with 459 clusters and 15 282 galaxies, we apply the Jeans analysis to get the velocity anisotropy profile of different galaxy populations. The results suggest that populations with a high rate of star formation, Star Forming, AGN and Transition, are characterized by more radial orbits when compared with the Quiescent population. Furthermore, these three populations have high projected velocity dispersions and, except for the AGN category, avoid central regions of clusters. These results suggest that populations Star Forming, AGN and Transition have been accreted more recently than other classes, being therefore characterized by more radial orbits and found (except the AGN category) in general in the clusters' outskirts. The presence of star formation and nuclear activity suggests that the environmental processes have still not being able to remove completely the gas from these populations.

Resumo. Galáxias possuem diferentes formatos e propriedades, além de uma tendência natural de se aglomerarem gravitacionalmente para formar grupos e aglomerados. Atualmente sabe-se que o ambiente de aglomerados pode modificar a morfologia e as propriedades das galáxias através de diversos processos. Desse modo, espera-se que haja uma relação entre a evolução orbital de uma população e o seu estado de relaxamento no aglomerado. Consequentemente, estudar as órbitas de galáxias pode nos fornecer informações sobre os processos ambientais que estão ocorrendo no ambiente intra-aglomerado. Neste trabalho, utilizando uma amostra contendo 459 aglomerados e 15 282 galáxias, aplicamos a análise de Jeans para obter os perfis de anisotropia de velocidades de diferentes populações de galáxias. Os resultados encontrados sugerem que as populações com maiores taxas de formação estelar, *Star Forming*, AGN e Transição, são caracterizadas por órbitas mais radiais, quando comparadas com a população Quiescente. Além disso, essas três populações possuem altas dispersões de velocidades projetada e, exceto para a categoria AGN, evitam as regiões centrais do aglomerado. Nossos resultados sugerem que as populações *Star Forming*, AGN e Transição foram acretadas mais recentemente que as demais, sendo, desse modo, caracterizadas por órbitas mais radiais e encontradas preferencialmente (exceto pela categoria AGN) na periferia dos aglomerados. A presença de formação estelar e atividade nuclear sugere que os processos ambientais ainda não foram capazes de remover completamente o gás dessas populações.

Keywords. Galaxies: clusters: general – Galaxy: kinematics and dynamics – Galaxy: evolution

1. Introduction

The orbital profile of galaxies in clusters gives us information about their evolution. We expect galaxies that are infalling into clusters to have more radial orbits when compared to galaxies that have resided longer therein. Furthermore, we know that the environment of clusters can affect the morphology and properties of the galaxies through several mechanisms (e.g. Moore, Lake & Katz 1998; Kauffmann et al. 2004; Weinmann et al. 2006). These mechanisms act on different timescales and are effective in different regions of the clusters (e.g. Treu et al. 2003; Boselli & Gavazzi 2006; Oman et al. 2021). Thus, we can study how these mechanisms affect different galaxy populations by analyzing the orbits of these populations.

To the present date, the literature has been unable to draw a uniform picture on the orbital profile of different populations of galaxies. Some authors find that star forming galaxies are characterized by more radial orbits when compared to quiescent galaxies (see e.g. Lotz et al. (2019), Biviano et al. (2021)). However, some works do not find differences in the orbital profile of star forming and quiescent galaxies, or between late-type and early-type galaxies (e.g. Hwang & Lee 2008; Biviano et al. 2013). Most of these works use a binary classification scheme, i.e. only two classes of galaxies are considered (e.g. Hwang & Lee 2008; Biviano et al. 2013; Lotz et al. 2019). Therefore, more studies are needed, especially when a more comprehensive galaxy classification is used, to better understand the relationship between galaxy population and orbital profiles.

The orbital characterization of galaxy clusters have usually been performed using the Jeans analysis. For a spherically symmetric cluster, the spherical Jeans equation can be written as

$$\frac{d(\nu\overline{v_r^2})}{dr} + 2\beta\frac{\nu\overline{v_r^2}}{r} = -\nu\frac{GM}{r^2}. \quad (1)$$

The observable profiles of line-of-sight (hereafter, LOS) velocity dispersion $\sigma_P(R)$ and the projected numerical density $I(R)$ are linked by

$$\sigma_P^2(R)I(R) = 2\int_R^\infty \nu(r)\overline{v_r^2}(r)\left(1-\beta(r)\frac{R^2}{r^2}\right)\frac{rdr}{\sqrt{r^2-R^2}}. \quad (2)$$

In these equations, $\nu(r)$ is the galaxy number density profile, $M(r)$ is the cluster mass profile, $v_r(r)$ is the radial component of the velocity profile and $\beta(r)$ is the anisotropy profile, defined as

$$\beta(r) = 1 - \frac{\overline{v_\theta^2} + \overline{v_\phi^2}}{2\overline{v_r^2}}, \quad (3)$$

where $\overline{v_\theta^2}$, $\overline{v_\phi^2}$ and $\overline{v_r^2}$ are the mean squared components of the velocity (Binney & Tremaine 2008). Isotropic orbits have $\beta(r) =$

0, radial orbits have $\beta(r) = 1$, and tangential orbits have $\beta(r) \to -\infty$.

In this work, we obtain the $\beta(r)$ profile for four populations of galaxies, classified with respect to the main ionizing source of the gas as obtained with optical diagnostic diagrams applied to a sample of 15 282 galaxies in 459 clusters from the Tempel, Tago & Liivamägi (2012) catalog.

2. Methodology

2.1. Sample

We used the sample of groups and clusters of galaxies from the Tempel, Tago & Liivamägi (2012) catalog, which is based on the 8th data release of the Sloan Digital Sky Survey (SDSS) (Aihara et al. 2011). This catalog comprises 576 493 galaxies ($12.5 \leq m_r \leq 17.77$) in 77 858 groups in the redshift range $0.009 \leq z \leq 0.2$.

To avoid highly disturbed, dynamically young clusters, we have selected only those clusters with no significant substructures, as evaluated by a 3-D κ test (Colless & Dunn 1996), with twenty or more confirmed members, thus obtaining 459 clusters and 15 282 galaxies.

2.2. Galaxy Classification

Using the CasJobs[1] platform we obtained the fluxes and equivalent widths of the optical emission lines (Hα, Hβ, [NII]λ6584 and [OIII]λ5007) as derived by Thomas et al. (2013) (and available as the "emissionLinesPort" table).

Galaxies are then classified into categories according to the main ionizing source of the gas, using simultaneously criteria from both BPT (Baldwin & Phillips 1981) and WHAN (Cid Fernandes et al. 2011) diagnostic diagrams. We consider four categories, namely: Star Forming (SF), Active Galactic Nuclei (AGN), Transition (T), and Quiescent (Q) galaxies. Galaxies are considered SF/AGN/T if they are located below the "Kauffmann" (Kauffmann et al. 2003) dividing line in the BPT diagram, above the "Kewley" (Kewley et al. 2006) line in the BPT diagram or between these two lines respectively, and if the WHAN diagram confirms that the gas ionization is not due to hot, low-mass evolved stars (HOLMES), i.e. $W_{\mathrm{H}\alpha} > 3$ Å (Cid Fernandes et al. 2011). Galaxies with $W_{\mathrm{H}\alpha} < 3$ Å are classified as Quiescent.

Some galaxies could not be classified by this method, due to the absence of the flux measurement of at least one of the emission lines necessary for the construction of any of the diagnostic diagrams. For these objects, we use a second set of criteria based only on the emission line measurements available for each galaxy. The criteria used were:

- If the galaxy lacks [OIII], Hβ or [NII] measurements, it is classified as Quiescent (Q) if $W_{\mathrm{H}\alpha} < 3$ Å, or Unclassifiable (U) otherwise.
- If the galaxy lacks Hα measurements, we classify it as a Quiescent galaxy if its [NII] equivalent width is lower than the 5% percentile of the distribution of equivalent widths of this same line among the entire set of Star Forming, AGN and Transition objects, or Unclassifiable (U) otherwise.

[1] https://skyserver.sdss.org/casjobs/

2.3. Ensemble cluster

The number of confirmed members with spectroscopic information per cluster does not allow to obtain individual profiles of mass and velocity anisotropy for each cluster. In order to circumvent this issue, we investigate the full sample of galaxies as if they belonged to a single cluster. This was performed by stacking our clusters, creating a so-called *ensemble cluster*. The projected radius and the LOS velocity of each galaxy were normalized by its parent cluster virial radius and velocity dispersion, respectively (see e.g. Katgert, Biviano & Mazure (2004), Biviano & Poggianti (2009) and Mamon et al. (2019)). The normalization makes the $\sigma_P(R)$ profile dimensionless, and the mass profile will be defined except by a multiplicative factor which depends on the virial radius and the velocity dispersion typical of the clusters in our sample.

2.4. Radial profiles

The application of the Jeans analysis depends on two main observable profiles, the LOS velocity dispersion profile $\sigma_P(R)$ and the galaxy projected numerical density profile $I(R)$. We obtained these profiles for our ensemble cluster separately for each galaxy class. The LOS velocity dispersion σ_P was derived from the interquartile range, i.e.

$$\sigma_P(R) = \frac{perc(75) - perc(25)}{1.349}, \tag{4}$$

where $perc(x)$ represents the x percentile of the distribution of velocity values. The velocity dispersion was calculated in radial bins to create a radial profile $\sigma_P(R)$. For each galaxy class, we used radial bins with a fixed number of galaxies instead of a fixed radial distance.

To calculate the projected numerical density profile, we count the number of galaxies inside a ring with inner radius R and outer radius $R+dR$. The value of $I(R)$ in the radial distance $R + dR/2$ is defined by the ratio

$$I(R) = \frac{N}{A}, \tag{5}$$

where N and A represent, respectively, the number of galaxies inside the ring and the area of the ring. The uncertainties in $I(R)$ are given by

$$\sigma_I(R) = \frac{\sqrt{N}}{A}. \tag{6}$$

In order to reduce the bin-to-bin variations due to random noise, we fit analytical functions to the measured radial profiles. To fit the $\sigma_P(R)$ profile, we use the following equation

$$\sigma_P(R) = a\left(1 - e^{-(R+d)/b}\right)(1 + c(R + d)^e), \tag{7}$$

which was found to do a good job in describing the overall shape of these profiles in our tests. The $I(R)$ profile was fit using one of the following profiles:

- a generalized Sérsic model (Sersic 1968):

$$I(R) = \exp\left(a + d(R + b)^c\right),$$

- a generalized King model (Adami et al. 1998):

$$I(R) = I_0\left(\frac{1}{1 + (R/R_s)^2}\right)^{\alpha}.$$

2.5. Mass profile

To obtain the mass profile $M(r)$ of our ensemble cluster, it is necessary to make some assumption about the shape of $\beta(r)$ or $\overline{v_r^2}(r)$. Katgert, Biviano & Mazure (2004) argue that quiescent galaxies, in general, have orbital configurations closer to equilibrium and, therefore, can be characterized with a good approximation by $\beta(r) = 0$. We use this same assumption to constrain the orbital profile of our Quiescent population and obtain the $M(r)$ profile of the ensemble cluster.

Firstly, we fit the observed profiles of $\sigma_P(R)$ and $I(R)$ of the Quiescent population using the analytical expressions described in the previous section. The radial numerical density profile $\nu(r)$ is then obtained from

$$\nu(r) = -\frac{1}{\pi}\int_r^\infty \frac{dI}{dR}\frac{dR}{\sqrt{R^2 - r^2}}. \tag{8}$$

In the special case $\beta(r) = 0$, Eq. 2 can be rewritten

$$\overline{v_r^2}(r) = -\frac{1}{\pi\nu(r)}\int_r^\infty \frac{d[I(R)\times\sigma_P^2(R)]}{dR}\frac{dR}{\sqrt{R^2 - r^2}}, \tag{9}$$

allowing us to solve for $\overline{v_r^2}(r)$ using the $\nu(r)$, $\sigma_P(R)$ and $I(R)$ profiles (see e.g. Katgert, Biviano & Mazure (2004)). Finally, the mass profile follow from the Jeans equation in spherical coordinates (1),

$$M(<r) = -\frac{r^2}{G\nu}\frac{d(\nu\overline{v_r^2})}{dr}. \tag{10}$$

2.6. Velocity anisotropy profile

Using the obtained mass profile, we performed an anisotropy inversion, following the method of Solanes & Salvador-Sole (1990), to obtain the $\beta(r)$ profile of the remaining populations. We started by defining the following functions

$$\Psi(r) = -G\frac{M(<r)\nu(r)}{r^2}, \tag{11}$$

$$H(R) = \frac{I(R)\sigma_P^2(R)}{2}, \tag{12}$$

and

$$K(r) = 2\int_r^\infty H(x)\frac{xdx}{\sqrt{x^2 - r^2}}. \tag{13}$$

As shown by Biviano & Katgert (2004), $\beta(r)$ and $\overline{v_r^2}(r)$ can be expressed in terms of the functions $\Psi(r)$ and $K(r)$ through the pair of equations

$$[3 - 2\beta(r)]\times\overline{v_r^2}(r) = -\frac{1}{\nu(r)}\int_r^\infty \Psi(x)dx - \frac{2}{\pi r\nu(r)}\frac{dK(r)}{dr}, \tag{14}$$

and

$$\begin{aligned}\beta(r)\overline{v_r^2}(r) =& \frac{1}{\nu(r)r^3}\int_0^r x^3\Psi(x)dx + \frac{1}{\pi r\nu(r)}\frac{dK(r)}{dr}\\ &- \frac{3K(r)}{\pi r^2\nu(r)} + \frac{3}{\pi r^3\nu(r)}\int_0^r K(x)dx.\end{aligned} \tag{15}$$

Table 1. Number of galaxies classified in each category (top row) and their corresponding percentage (bottom row).

SF	AGN	T	Q	U
4403	329	1233	9226	91
28.81%	2.15%	8.07%	60.37%	0.60%

3. Results and Discussions

3.1. Galaxy classification

The number of galaxies classified in each category and their corresponding percentage is shown in Tab. 1. Figure 1 shows the location of the galaxies in the BPT and WHAN diagrams and their respective classes, indicated by different colors. In the middle pannel of Fig. 1, we can see that there is a large fraction of objects located in the AGN and Transition regions of the BPT diagram, but that are actually ionized by HOLMES and were therefore classified as Quiescent galaxies by us. Also, there is a large fraction of galaxies in the AGN region of the WHAN diagram that are classified as Star Forming or Transition, when we use a mixed classification. This results in a strong reduction ($\sim$ 87% and $\sim$ 56%, respectively) in the number of AGN and Transition galaxies we would have obtained using only one of these diagrams. The classification system we have used allows us to remove from these classes objects whose ionization source do not involve an active nucleus.

3.2. Radial profiles

The measured $I(R)$ and $\sigma_P(R)$ profiles are shown for each category in Fig. 2 and Fig. 3, respectively. Figure 2 shows that the number density profiles for Quiescent galaxies and AGN are strongly peaked in the cluster centers. On the other hand, galaxies of the Star Forming and Transition populations present a "plateau" towards the central region, roughly inside the ensemble cluster virial radius. In Fig. 3 we see that the Star Forming, AGN and Transition categories have higher values of velocity dispersion in almost all radii when compared to the Quiescent population. These results show us that categories composed of galaxies with a more intense gas ionization signature tend to have higher velocity dispersion and avoid the central regions of clusters. On the other hand, Quiescent galaxies tend to concentrate in the central regions and present low-velocity dispersion. It is important to note that the results for the AGN population are noisy due to the sample size and need to be confirmed with larger samples.

3.3. Mass profile

The mass profile obtained for our ensemble cluster is shown in the Fig. 4. The $M(r)$ profile grows as we move to outer regions, as expected. However, we do not see a flattening of the profile at large radii, as would be expected physically. This may indicate that the dark matter halo extends to greater distances than can be mapped with the distribution of galaxies. Furthermore, this could also be due to extrapolations in the $\sigma_P(R)$ and $I(R)$ profiles in higher values of R, since we do not know if they physically represent the profiles in these regions. It is important to emphasize that the $M(r)$ profile presents two growth trends, one internal and the other external. The behavior observed in the external region seems to agree with that obtained by Katgert, Biviano & Mazure (2004), although the internal trend observed by us is not observed by these authors.

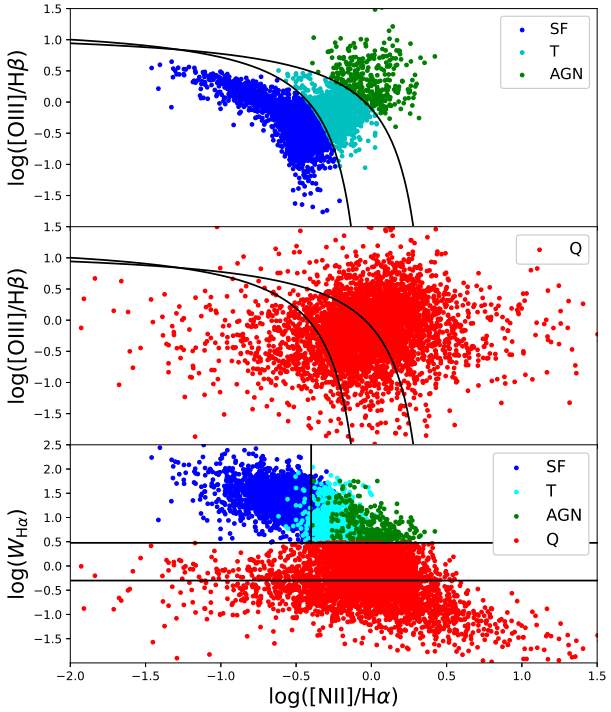

Figure 1. Positions, in the BPT (top and middle panels) and WHAN (bottom panel) diagrams, of the 10831 galaxies in the sample for which the emission line fluxes of Hα, Hβ, [NII]λ6584 and [OIII]λ5007 were available in the SDSS database. Different galaxy classes are indicated by different colors (see insets). In the top and middle panels, the dividing lines are from Kauffmann et al. (2003) and Kewley et al. (2006); the dividing lines in the bottom panel come from Cid Fernandes et al. (2011).

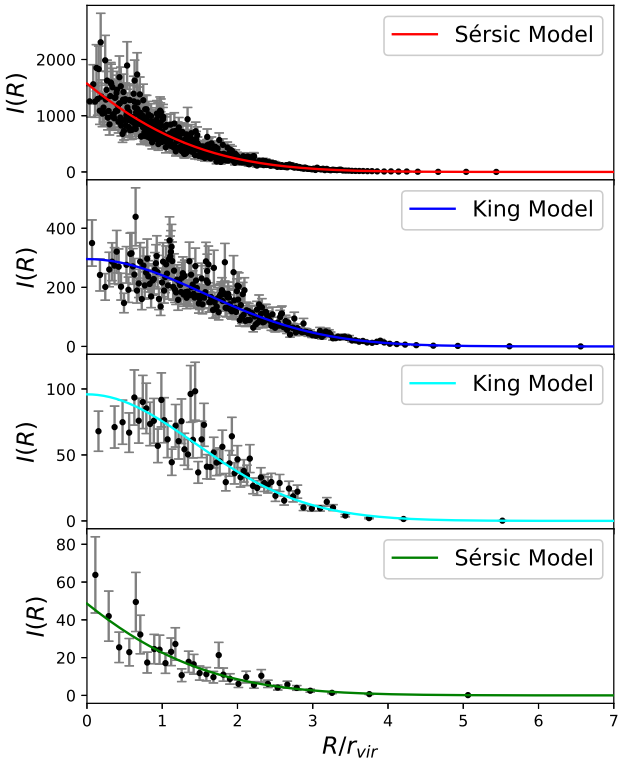

Figure 2. Projected radial profiles $I(R)$ of galaxies in the four ionization classes, namely Quiescent (first panel), SF (second panel), T (third panel) and AGN (fourth panel). In the figure legend is shown the analytic function adjusted to the observed profile (Quiescent in red, SF in blue, T in cyan, AGN in green).

3.4. Velocity anisotropy profile

The $\beta(r)$ profile obtained for the four categories is shown in Fig. 5. The $\beta(r)$ profile for the Quiescent population was obtained as a means of verifying the consistency of the $M(r)$ profile, and, as we can see, the profile obtained is in good agreement with the assumption $\beta(r) = 0$ used to obtain the $M(r)$.

Analyzing the Fig. 5, we see that the Star Forming, AGN, and Transition populations have more radial orbits (larger values of $\beta(r)$) when compared to the Quiescent population. These results show that galaxies with higher star formation and/or host an optical AGN have more radial orbits when compared to quiescent galaxies. This happens mainly in the outermost parts of the clusters since in the inner regions all categories tend to present more isotropic orbits.

We interpret these results as the signature of galaxy populations that are just entering the cluster environment or have been accreted more recently than the bulk of the Quiescent population. Therefore, they tend to have more radial orbits, larger velocity dispersions, and to be less concentrated in the central regions of the clusters. Likewise, as they may have just arrived in the clusters' environments, there has not been enough time for their gas content to have been efficiently removed, allowing such galaxies to appear to us as belonging to gas-rich / AGN populations. On the other hand, populations that have resided longer in the cluster will present orbits closer to equilibrium, low-velocity dispersion, and present high concentrations in the central regions. In addition, they will also have had their gas content removed by environmental mechanisms, appearing to us as quiescent galaxies.

4. Conclusions

In this work, we analyzed the velocity anisotropy profile for four galaxy populations (Star Forming, Quiescent, Transition, and AGN), obtained after applying an optical classification, using the BPT and WHAN diagnostic diagrams, to a sample containing 15 282 galaxies belonging to 459 clusters. The main conclusions reached, are summarized below:

- Populations that have a more intense optical ionized gas signature tend to present more radial orbits relative to quiescent galaxies, especially on the outskirts of clusters.
- The above result suggests that the Star Forming and Transition populations are less virialized than the Quiescent population in the cluster.
- The AGN population also appears to be less virialized than the Quiescent population, but the results are very uncertain, due to the fact that our optical AGN sample is very small.

A more detailed study, where uncertainties in the $\beta(r)$ profiles are estimated, becomes necessary to confirm such conclu-

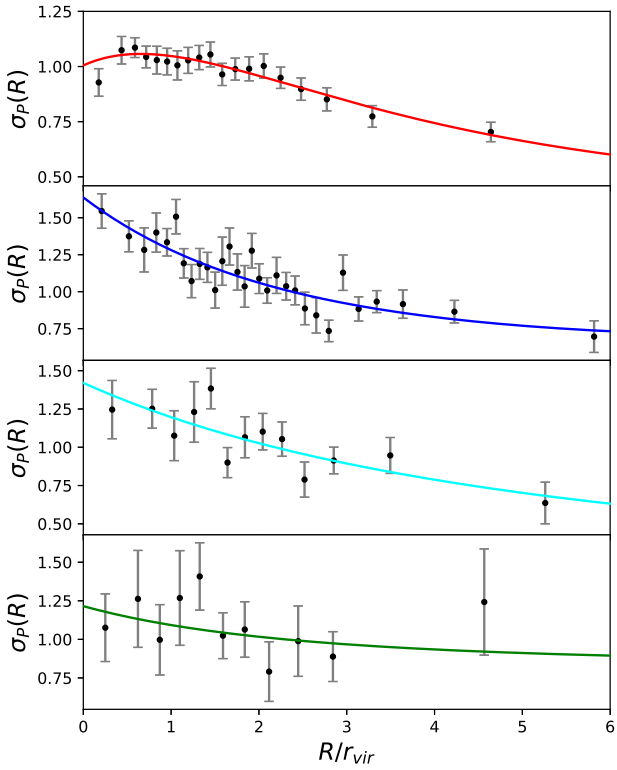

Figure 3. Radial profiles of $\sigma_P(R)$ of galaxies in the four ionization classes. The order of the panels and the colors of the fitted analytical profiles are the same as in 2.

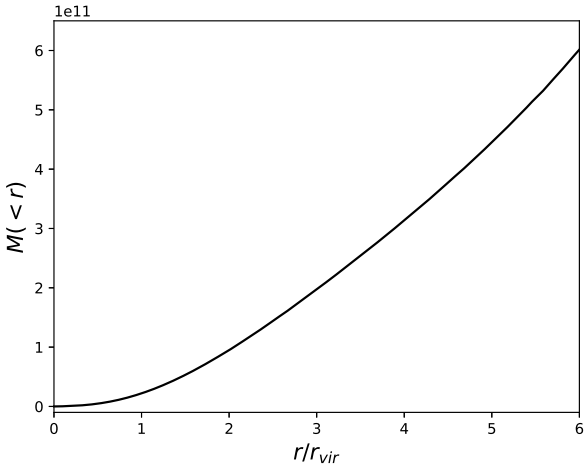

Figure 4. $M(r)$ profile obtained for our ensemble cluster by applying Jeans analysis to the Quiescent population. The mass units are given in terms of the normalization of radial distances and LOS velocities.

sions. In addition, a larger sample for the AGN category is necessary, in order to better restrict the results obtained.

Acknowledgements. This study was financed in part by the Coordenação de Aperfeiçoamento de Pessoal de Nível Superior – Brasil (CAPES) – Finance Code 001.

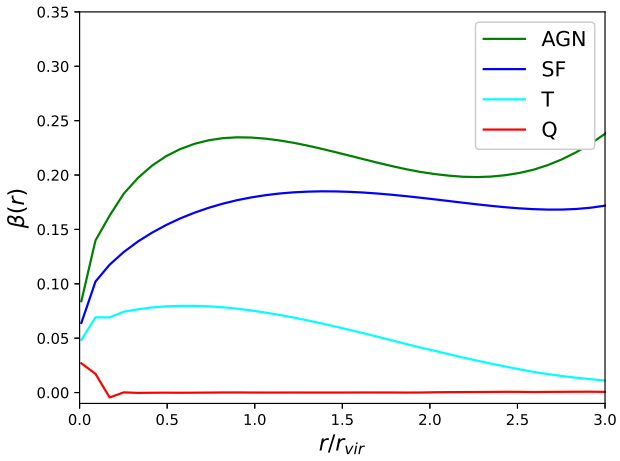

Figure 5. Radial profiles for $\beta(r)$, obtained using $M(r)$ profile. The representative color of each population can be identified in the figure legend.

References

Adami, C., Mazure, A., Katgert, P., Biviano, A. 1998, A&A, 336, 63
Adhikari, S., Dalal, N., More, S., Wetzel, A. 2019, ApJ, 878, 9
Aihara, H., et al. 2011, ApJS, 193, 29
Baldwin J. A., Phillips, M. M., Terlevich, R. 1981, PASP, 93, 5
Binney, J., Tremaine, S. 2008, Galactic Dynamics, (Princeton: Princeton University Press)
Biviano, A., Katgert, P. 2004, A&A, 424, 779
Biviano, A., Poggianti, B. M. 2009, A&A, 501, 419
Biviano, A., et al. 2013, A&A, 558, A1
Biviano, A., et al. 2021, A&A, 650, A105
Boselli, A., Gavazzi, G. 2006, PASP, 118, 517
Cid Fernandes, R., Stasińska, G., Mateus, A., Vale Asari, N. 2011, MNRAS, 413, 1687
Colless, M., Dunn, A. M. 1996, ApJ, 458, 435
Hwang, H. S., Lee, M. G. 2008, ApJ, 676, 218
Katgert, P., Biviano, A., Mazure, A. 2004, ApJ, 600, 657
Kauffmann, G., et al. 2003, MNRAS, 346, 1055
Kauffmann, G., White, S. D. M., Heckman, T. M., Ménard, B., Brinchmann, J., Charlot, S., Tremonti, C., Brinkmann, J. 2004, MNRAS, 353, 713
Kewley, L. J., Groves, B., Kauffmann, G., Heckman, T. 2006, MNRAS, 372, 961
Lotz, M., Remus, R.-S., Dolag, K., Biviano, A., Burkert, A. 2019, MNRAS, 488, 5370
Mamon, G. A., Cava, A., Biviano, A., Moretti, A., Poggianti, B., Bettoni, D. 2019, A&A, 631, A131
Moore, B., Lake, G., Katz, N. 1998, ApJ, 495, 139
Oman, K. A., Bahé, Y. M., Healy, J., Hess, K. M., Hudson, M. J., Verheijen, M. A. W. 2021, MNRAS, 501, 5073
Sersic, J. L. 1968, Atlas de Galaxias Australes, (Cordoba: Observatorio Astronomico)
Solanes, J. M., Salvador-Sole, E. 1990, A&A, 234, 93
Tempel, E., Tago, E., Liivamägi, L. J. 2012, A&A, 540, A106
Thomas, D., et al. 2013, MNRAS, 431, 1383
Treu, T., Ellis, R. S., Kneib, J.-P., Dressler, A., Smail, I., Czoske, O., Oemler, A., Natarajan, P. 2003, ApJ, 591, 53
van der Marel, R. P. 1994, MNRAS, 270, 271
Weinmann, S. M., van den Bosch, F. C., Yang, X., Mo, H. J. 2006, MNRAS, 366, 2